


Deep-red electro-fluorescence based on an  
excimer emission with hot-exciton channels†Ying Gao,<sup>‡a</sup> Mingming Yao,<sup>‡,b</sup> Changjiang Zhou,<sup>c</sup> Haichao Liu,<sup>a</sup> Shi-Tong Zhang<sup>\*a</sup>  
and Bing Yang <sup>\*a</sup>Cite this: *J. Mater. Chem. C*, 2022,  
10, 4579Received 14th October 2021,  
Accepted 16th December 2021

DOI: 10.1039/d1tc04920h

rsc.li/materials-c

Red and deep-red fluorescent materials are broadly applied in many fields, such as organic light emitting diodes (OLEDs), biological imaging and night-vision devices. In this work, we designed and synthesized two orange to red emissive donor–acceptor (D–A) materials, DMAC-NZP and DMAC-NZC, in which DMAC-NZC possesses an extra cyano group. The DMAC-NZC aggregate demonstrates a large red-shift of 60 nm compared with DMAC-NZP, which can be assigned to the formation of discrete dimer and excimer emissions in its single crystal and neat films, respectively, upon cyano-substitution. Both DMAC-NZC and DMAC-NZP exhibit a maximum external quantum efficiency (EQE<sub>max</sub>) of over 4% and a very small efficiency roll-off in doped OLEDs. More importantly, the non-doped OLEDs of DMAC-NZC show deep-red electrofluorescence at 688 nm with a considerably high exciton utilization efficiency (EUE) of 55%–82%. This work not only gives a new functional group for the construction of deep-red pure organic efficient excimer materials, but also further verifies that the “hot exciton” theory can also be effective in the excimer-based OLEDs.

## Introduction

Red and deep-red fluorescent materials have received tremendous scientific and commercial attention over the last few decades, owing to their applications in organic light-emitting diodes (OLEDs), biological imaging, night-vision devices and so forth.<sup>1–6</sup> Generally, constructing the donor–acceptor structure and extending  $\pi$ -conjugation are the most frequently applied

approaches to achieve red fluorescent materials.<sup>7,8</sup> However, high-efficiency red light-emitting materials are still rare compared with green and blue emissive materials due to the resonance of the vibrational wave function of the excited state and the ground state, which may accelerate the non-radiative transitions and cause a low photoluminescence quantum yield (PLQY). Another commonly used approach to realize largely red-shifted emission is the intermolecular aggregation, especially the  $\pi$ - $\pi$  interaction. However, it is still important to prevent the aggregation caused quenching (ACQ) that causes a bad decrease of the PLQY. Overall, it is still challenging to pave the way for realizing efficient red-emissive materials and their aggregates.

Despite the fact that the aggregates, especially the excimer and exciplex, that are used are believed to be of low-efficiencies, recently, our group have reported a series of highly efficient excimer fluorescent materials.<sup>9–11</sup> For example, with systematically regulated side-group substitutions, the optimized structure 2-(anthracen-9-yl) thianthrene (2-TA-AN) exhibits a green excimer emission at 526 nm with a considerably high PLQY of 80% compared with its deep-blue, but low-efficiency monomer emission (424 nm, PLQY = 33%).<sup>12</sup> However, the present excimer is that the molecular structure of these efficient excimers is limited to anthracene derivatives, which can only produce a green emission. To date, there are almost no reports on the structures of efficient red-emissive excimers, let alone electroluminescence based on red-emissive excimers.

In this work, we reported two red-emissive donor–acceptor materials **DMAC-NZC** and **DMAC-NZP** using 9,9-dimethyl-10-phenyl-9,10-dihydroacridine (DMAC) and naphtho[2,3-*c*]-[1,2,5]thiadiazole (NZ) as donor and acceptor moieties, respectively (Scheme 1).<sup>13</sup> Compared to **DMAC-NZP**, an extra cyano-group is involved in **DMAC-NZC**, which forms a pair of hydrogen bonds as the “interlock” of two adjacent **DMAC-NZC** molecules, generating typical discrete dimers with a large red-shift compared with the **DMAC-NZC** monomer (66 nm) and the **DMAC-NZP** aggregate (60 nm). The non-doped OLED of **DMAC-NZC** demonstrates deep-red electroluminescence (EL) at 688 nm with a maximum external quantum efficiency

<sup>a</sup> State Key Lab of Supramolecular Structure and Material, Institute of Theoretical Chemistry, College of Chemistry, Jilin University, Changchun, P. R. China.

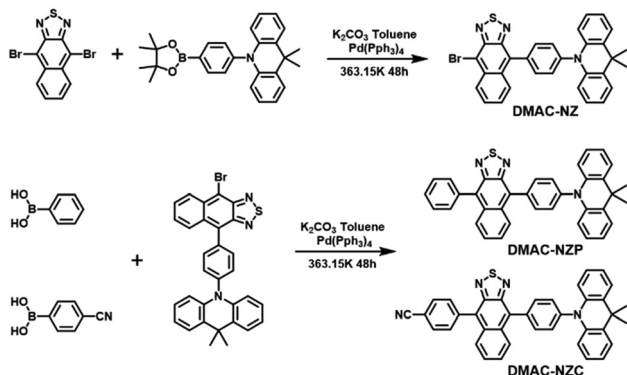
E-mail: stzhang@jlu.edu.cn, yangbing@jlu.edu.cn

<sup>b</sup> Jilin OLED Material Tech Co. Ltd, Changchun, P. R. China

<sup>c</sup> College of Chemical Engineering, Zhejiang University of Technology, Hangzhou, P. R. China

† Electronic supplementary information (ESI) available. CCDC 2115526 and 2115527. For ESI and crystallographic data in CIF or other electronic format see DOI: 10.1039/d1tc04920h

‡ Co-authors.



Scheme 1 Structures and syntheses of **DMAC-NZC** and **DMAC-NZP**. Detailed synthesis processes and characterization data are shown in the ESI† (Fig. S14–S19).

(EQE<sub>max</sub>) of 0.7%, corresponding to a *Commission Internationale de l'Eclairage* (CIE) of (0.65, 0.34). More importantly, cyano-substitution also contributes to the reduced OLED rolling-off from **DMAC-NZC** (7%) to **DMAC-NZP** (18%), revealing the potential of deep-red, pure-organic excimer-emission OLEDs.<sup>14,15</sup>

## Results and discussion

The normalized absorption and photoluminescence (PL) spectra of **DMAC-NZC** and **DMAC-NZP** in different solvents are shown in Fig. 1. The absorption bands of **DMAC-NZC** and **DMAC-NZP** are all in the range of 375–550 nm, displaying broadband absorption that can be assigned to the intramolecular charge-transfer (CT) transition from the donor DMAC to the acceptor NZ unit, which is the key necessity of the possible efficient triplet-to-singlet reverse intersystem crossing (RISC) process for OLEDs. Further proof for the formation of strong CT characteristics is that, in Fig. 1b, different from the typical solvatochromic PL spectra of the molecular CT structure, an obvious “blue-shift” can be observed in

acetonitrile solutions of the two materials, which is essentially combined by the visible LE and the largely red-shifted, poorly quenched pure CT emission of the dual-emission caused by high solvent polarity.<sup>16–18</sup> Additionally, the diluted solutions, neat films and doped films of **DMAC-NZC** and **DMAC-NZP** all exhibit single-exponential PL decay, indicating that both of the two materials are not of traditional TADF properties (Table S1, ESI†).

Notably, although it seems that the introduction of the cyano-group does not make much difference to the **DMAC-NZC** and **DMAC-NZP** monomer emissions (diluted solutions and the doped films), the aggregates of **DMAC-NZC** and **DMAC-NZP** demonstrate quite different emission behaviours, including the light-colour and PLQY (Fig. 1b, c and Table 1). The neat powder and the single crystal of **DMAC-NZC** show a larger red-shift of near 60 nm compared with **DMAC-NZP**, which is in favour of better red purity. It should be noticed again that the aggregation in **DMAC-NZC** does not produce dual-emissions as in the large polarity solvents, which gives possibility for the fabrication of the non-doped deep-red OLEDs and, more importantly, implies that, distinguishing from **DMAC-NZP** and other CT or hybrid locally excited and charge-transfer (HLCT) materials, the large red-shift of the **DMAC-NZC** aggregate is not induced by polar circumstances.<sup>19–22</sup> The molecular structures and packing modes of their single crystals can illustrate the structural reason why **DMAC-NZC** can demonstrate better red purity. As shown in Fig. 2, the **DMAC-NZC** single crystal mainly contains a face-to-face dimeric stacking between two NZ moieties with a  $\pi$ -overlap of 61% (Fig. S13b, ESI†). Such a large  $\pi$ -overlap in face-to-face dimeric stacking of NZ units manifest a strong  $\pi$ - $\pi$  interaction, which contributes to the largely red-shifted fluorescence of **DMAC-NZC**. Furthermore, the cyano-group makes great contributions to the formation of the face-to-face dimer. In Fig. 2, the intermolecular C-H $\cdots$ N interactions can serve as the “interlock” of two adjacent **DMAC-NZC** molecules and form discrete dimers in the whole crystal, making a stable red-shifted emission. In comparison, this regularly arranged dimer cannot be found

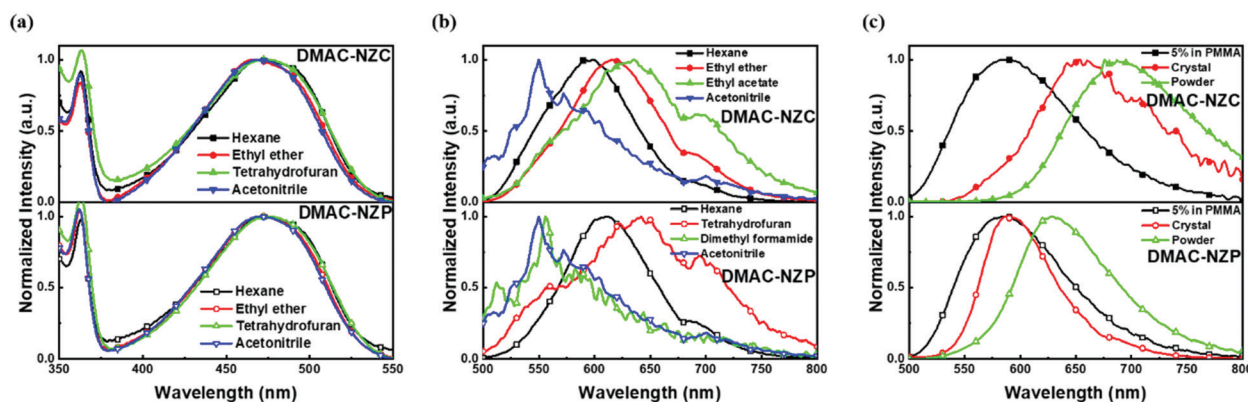
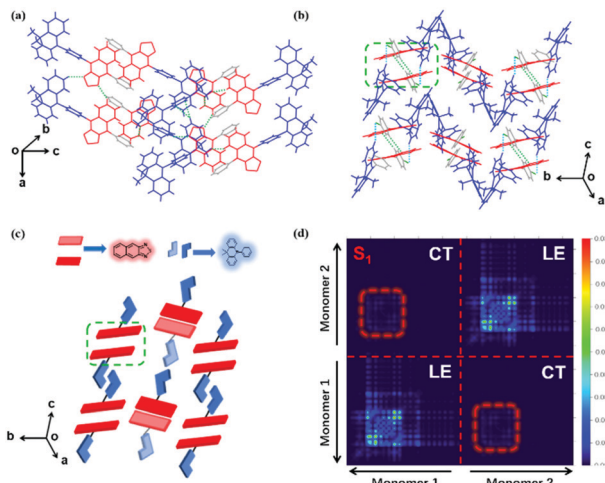


Fig. 1 Photophysical properties of the diluted solutions and solid-states of **DMAC-NZC** and **DMAC-NZP**. (a) Absorption spectra of **DMAC-NZC** and **DMAC-NZP** in diluted solutions. (b) Photoluminescence (PL) spectra of **DMAC-NZC** and **DMAC-NZP** in diluted solutions. (c) PL spectra of **DMAC-NZC** and **DMAC-NZP** in 5% PMMA film, single crystals and neat powders. In addition, the concentration of the solution is  $<10^{-5}$  mol L<sup>-1</sup> to guarantee the mono-dispersity. Notably, the “shoulder” peaks at  $\sim 680$  nm in (b) are assigned to the grating defects of the instrument.

**Table 1** PLQYs of **DMAC-NZC** and **DMAC-NZP** in the powder, crystal and 5% PMMA film

Materials/PLQY (%)	Powder	Crystal	5% Doped film in PMMA
<b>DMAC-NZC</b>	4.3	3.2	71
<b>DMAC-NZP</b>	35	5.7	75



**Fig. 2** (a and b) Crystal structures of **DMAC-NZP** and **DMAC-NZC**, respectively. (c) Schematic diagram of the discrete NZ dimer formation. (d) Transition density matrix color-filled map of the  $S_1$  state of the **DMAC-NZC** dimer. The molecular conformation and crystal packing information are obtained by single-crystal X-ray diffraction (XRD).

in **DMAC-NZP**; instead, only C-H... $\pi$  interactions can be found in its crystal structure, which is the reason why there is a density matrix (TDM) of the  $S_1$  excited state of **DMAC-NZC** using the Multiwfn package.<sup>23</sup> In Fig. 2d, it can be observed that the interchange (or intermolecular CT) exists in the  $S_1$  excited state of **DMAC-NZC**, which is an obvious indicator of the excimer formation. Additionally, it should be noted that due to the substitution of the electron donor, the lifetime of the **DMAC-NZC** crystal is even shorter than its dispersed film (Table S1, ESI<sup>†</sup>), which is quite different to the traditional excimer emissions and more suitable for the fabrication of a non-doped OLED.

The two materials both possess satisfactory thermal stabilities of  $> 120$  °C glass transition temperature ( $T_g$ ) and  $> 350$  °C thermal deposition temperature ( $T_d$ ), which enable their further application in electroluminescence (EL) (Fig. S4 and S5, ESI<sup>†</sup>). Moreover, the thermal stability of **DMAC-NZC** is better than that of **DMAC-NZP**, owing to the introduction of the cyano-group and stronger intermolecular interactions. The non-doped OLED performances of the two materials are summarized in Table 2. In particular, the OLED based on **DMAC-NZC** shows deep-red EL at 688 nm, corresponding to a *Commission Internationale de l'Eclairage* (CIE) coordinate of (0.65, 0.34), implying that the EL of the non-doped OLED of **DMAC-NZC** is originated from the excimer emission of its neat film (Fig. 3a). More importantly, it is worth noting that the efficiency rolling-off of both the doped and non-doped OLEDs based on **DMAC-NZC** are only near 7%, proving that the cyano-group substitution not only exhibits an obvious red-shift by the effective dimer formation, but also increases the stability of the films and OLEDs (Table 2).

Last but not least, the exciton utilization efficiencies (EUEs) of both the doped and non-doped OLEDs of **DMAC-NZC** and **DMAC-NZP** are all far superior compared to the 25% spin-statistics limit even if the light-out-coupling efficiencies ( $\eta_{out}$ ) of the glass substrate OLEDs are estimated as an upper limit of 30%, matching well with the “hot-exciton” model (Fig. 4 and Fig. S8, ESI<sup>†</sup>). We carried out density functional theory (DFT) and time-dependent DFT (TDDFT) calculations to demonstrate the mechanism of the exceeding EUEs of the two materials. As shown in Fig. 4a and b, the energy diagram of the two materials demonstrates the typical “hot-exciton” model, which should meet three typical demands:<sup>24–36</sup>

- (1) A large energy gap between  $T_2$  and  $T_1$  for forbidden internal conversion from  $T_2$  to  $T_1$ .
- (2) The CT excited state properties of  $T_2$  and  $S_2$ , and a small energy gap for efficient reverse intersystem crossing (RISC).
- (3) Considerable spin-orbit coupling (SOC) of  $T_2$  and  $S_2$  can also help boost the “hot-exciton” channel.

In Fig. 4, for the occasion of **DMAC-NZC** and **DMAC-NZP**, first, they both possess large  $T_1$  and  $T_2$  excited state energy gaps, which can block the internal conversion processes. Secondly, they both possess a small  $T_2$ – $S_2$  energy splitting, which can increase the RISC rate from  $T_2$  to  $S_2$ . Next, both for **DMAC-NZC** and **DMAC-NZP**, the natural transition orbitals

**Table 2** Non-doped and doped OLED performances of **DMAC-NZC** and **DMAC-NZP**

Emitter	$V_{on}$ (V)	$\lambda_{EL}$ (nm)	$CE_{max}$ (cd A <sup>-1</sup> )	$PE_{max}$ (lm W <sup>-1</sup> )	CIE (x,y)	$EQE_{max}/EQE_{100}/EQE_{1000}$ (%)	Max luminance (cd m <sup>-2</sup> )	Roll-off (%)	PLQY (%)	EUE (%)
NZC	3.1	688	0.32	0.16	0.65,0.34	0.70/0.62/0.65	1859	7.1	4.2	55–83
NZP	3.3	628	2.5	2.5	0.61,0.39	2.0/1.7/1.6	11 790	18	9.2	66–99
NZC (doped)	3.8	588	9.2	6.9	0.50,0.45	4.1/4.1/3.8	9612	7.1	47	29–44
NZP (doped)	3.2	612	6.9	6.8	0.58,0.41	4.0/3.9/3.4	15 820	17	28	47–71

$V_{on}$ : turn-on voltage;  $\lambda_{EL}$ : electro-luminous wavelength;  $CE_{max}$ : maximum luminous efficiency;  $PE_{max}$ : maximum power efficiency; CIE: Commission Internationale de l'Eclairage (CIE) coordinate;  $EQE_{max}/EQE_{100}/EQE_{1000}$ : maximum external quantum efficiency/EQE at 100 (cd m<sup>-2</sup>) luminance/EQE at 1000 (cd m<sup>-2</sup>); rolling-off: rolling-off =  $(EQE_{max} - EQE_{1000})/EQE_{max}$ ; EUE:  $EUE = (\gamma \times EUE \times \Phi_{PL}) \times \eta_{out}$ , where  $\gamma$  is the recombination efficiency of the injected electron and hole (generally identified as 100%);  $\Phi_{PL}$  is the PLQY of the emitter;  $\eta_{out}$  is the light out-coupling fraction, which is estimated as a range of 20%–30% for the glass substrates.

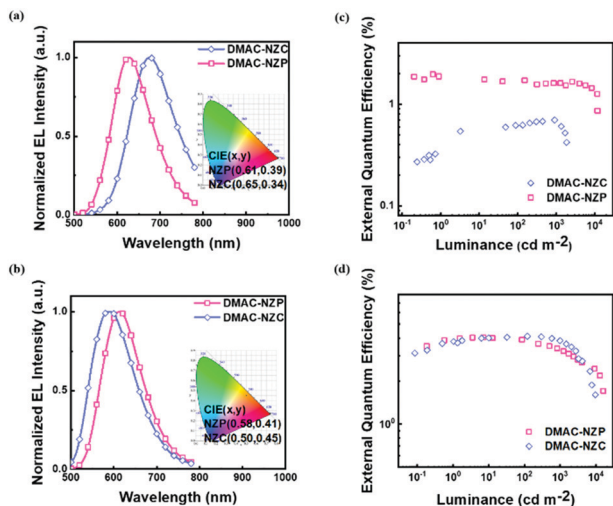


Fig. 3 OLED performances of **DMAC-NZC** and **DMAC-NZP**. (a and c) Electroluminescence spectra of **DMAC-NZC** and **DMAC-NZP** in non-doped OLEDs and doped OLEDs, respectively. (b and d) External quantum efficiency (EQE)-luminance diagrams of **DMAC-NZC** and **DMAC-NZP** in non-doped OLEDs and doped OLEDs, respectively. The OLED structures are ITO/HATCN(5 nm)/TPAC(20 nm)/TCTA(10 nm)/**DMAC-NZC** or **DMAC-NZP** or CBP:**DMAC-NZC** or CBP:**DMAC-NZP**(20 nm)/TPBi(40 nm)/LiF(1 nm)/Al(100 nm).

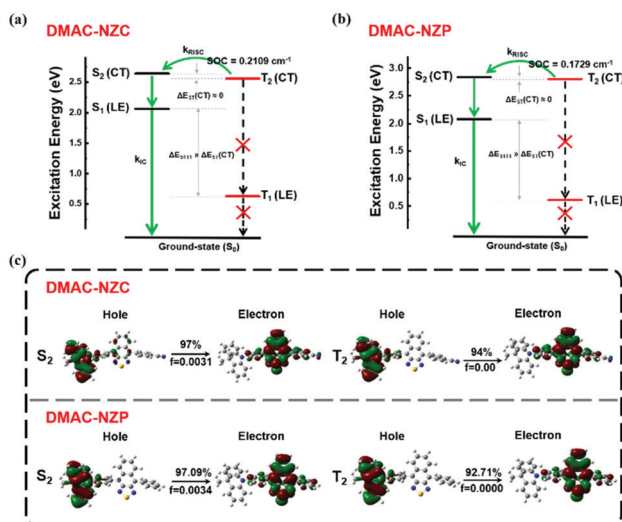


Fig. 4 Molecular simulation on the excited states of **DMAC-NZC** and **DMAC-NZP**. (a) The excitation energy level of **DMAC-NZC**. (b) The excitation energy level of **DMAC-NZP**. (c) The NTO of the  $S_2$  and  $T_2$  excited states of **DMAC-NZC** and the NTO of the  $S_2$  and  $T_2$  excited states of **DMAC-NZP**. The DFT and TDDFT calculations are carried out using the Gaussian 09 D.01 package using the hybrid function m062x under the 6-31g(d,p) level.<sup>37–40</sup>

(NTOs) of the  $S_2$  and  $T_2$  excited states show apparent CT state properties with separated hole and electron wave functions (Fig. 4c). Last but not least, the SOC rates between the  $T_2$  and  $S_2$  excited states of **DMAC-NZC** and **DMAC-NZP** are estimated as  $0.2109 \text{ cm}^{-1}$  and  $0.1792 \text{ cm}^{-1}$ , respectively. These values are

seemingly smaller than those of the metallic complexes or some room-temperature-phosphorescent organic materials that contain heavy atoms, but they can also afford efficient RISC according to the reported studies.<sup>41–45</sup> More importantly, the **DMAC-NZC** dimer can well inherit both the “hot-exciton” energy structure and the characteristic NTO of its monomer, which is identical to its boosting EUE of the non-doped OLED.

## Conclusions

In summary, we adapt the cyano-group as an auxiliary acceptor to further improve the color purity of red-emissive NZ based D–A derivatives. The cyano-substituted material **DMAC-NZC** demonstrates deep-red, excimer induced EL in the non-doped OLED, which is of 60 nm red-shift compared to the non-substituted **DMAC-NZP**. The structural reason that **DMAC-NZC** possesses largely red-shifted emission can be assigned to its discrete dimer formation, in which two C–H...N interactions between the cyano-group and the phenyl ring on the adjacent monomer serve as the interlocks. More importantly, the cyano-group is a conjugative electron donating moiety, which can also improve the PLQY. In addition, photo-physical characterization and theoretical calculations suggest that **DMAC-NZC** and **DMAC-NZP** are both HLCT materials with the “hot exciton” RISC channel, which contributes to high PLQYs and high exciton utilization in OLEDs. Overall, the introduction of the cyano-group could be an effective method to design the next-generation of cheaper, easily synthesized red and deep-red electro-fluorescent excimer materials.

## Author contributions

Ying Gao: Data curation, formal analysis, and writing – original draft. Mingming Yao: Data curation, formal analysis, and writing – original draft. Ying Gao and Mingming Yao contributed equally. Changjiang Zhou: Data curation, formal analysis, and writing – original draft. Haichao Liu: Data curation, formal analysis, and writing – original draft. Shi-Tong Zhang: Conceptualization, formal analysis, funding acquisition, writing – original draft, writing – review and editing, and supervision. Bing Yang: Funding acquisition, writing – review and editing, and supervision.

## Conflicts of interest

The authors declare that they have no known competing financial interests or personal relationships that could have appeared to influence the work reported in this paper.

## Acknowledgements

This work was supported by the National Natural Science Foundation of China (51803071, 51903031 and 91833304), the National Basic Research Program of China (2016YFB0401001) and the JLUSTR (2019TD-33).

## Notes and references

- N. Alifu, A. Zebibula, J. Qi, H. Zhang, C. Sun, X. Yu, D. Xue, J. W. Y. Lam, G. Li, J. Qian and B. Z. Tang, *ACS Nano*, 2018, **12**, 11282–11293.
- W. Ge, Y. Xu, C. Liu, W. Xu, Y. Zhang, W. Si, W. Zhao, C. Ou and X. Dong, *J. Mater. Chem. B*, 2021, **9**, 8300–8307.
- Z. He, Y. Gao, H. Zhang, Y. Xue, F. Meng and L. Luo, *Adv. Healthcare Mater.*, 2021, e2101056, DOI: 10.1002/adhm.202101056.
- Z. Sheng, B. Guo, D. Hu, S. Xu, W. Wu, W. H. Liew, K. Yao, J. Jiang, C. Liu, H. Zheng and B. Liu, *Adv. Mater.*, 2018, e1800766, DOI: 10.1002/adma.201800766.
- Q. Wan, R. Zhang, Z. Zhuang, Y. Li, Y. Huang, Z. Wang, W. Zhang, J. Hou and B. Z. Tang, *Adv. Funct. Mater.*, 2020, **30**, 2002057.
- S. Zhu, S. Herraiz, J. Yue, M. Zhang, H. Wan, Q. Yang, Z. Ma, Y. Wang, J. He, A. L. Antaris, Y. Zhong, S. Diao, Y. Feng, Y. Zhou, K. Yu, G. Hong, Y. Liang, A. J. Hsueh and H. Dai, *Adv. Mater.*, 2018, **30**, e1705799.
- Y. Shen, Z. Zhang, H. Liu, Y. Yan, S. Zhang, B. Yang and Y. Ma, *J. Phys. Chem. C*, 2019, **123**, 13047–13056.
- B. Situ, M. Gao, X. He, S. Li, B. He, F. Guo, C. Kang, S. Liu, L. Yang, M. Jiang, Y. Hu, B. Z. Tang and L. Zheng, *Mater. Horiz.*, 2019, **6**, 546–553.
- W. Jiang, Y. Shen, Y. Ge, C. Zhou, Y. Wen, H. Liu, H. Liu, S. Zhang, P. Lu and B. Yang, *J. Mater. Chem. C*, 2020, **8**, 3367–3373.
- H. Liu, Y. Shen, Y. Yan, C. Zhou, S. Zhang, B. Li, L. Ye and B. Yang, *Adv. Funct. Mater.*, 2019, **29**, 1901895.
- Q. Luo, L. Li, H. Ma, C. Lv, X. Jiang, X. Gu, Z. An, B. Zou, C. Zhang and Y. Zhang, *Chem. Sci.*, 2020, **11**, 6020–6025.
- H. Liu, Y. Gu, Y. Dai, K. Wang, S. Zhang, G. Chen, B. Zou and B. Yang, *J. Am. Chem. Soc.*, 2020, **142**, 1153–1158.
- T. Liu, L. Zhu, C. Zhong, G. Xie, S. Gong, J. Fang, D. Ma and C. Yang, *Adv. Funct. Mater.*, 2017, **27**, 1606384.
- A. Sharma, K. R. J. Thomas, K. K. Kesavan, I. Siddiqui, M. Ram Nagar and J.-H. Jou, *ACS Appl. Electron. Mater.*, 2021, **3**, 3876–3888.
- D. G. Congrave, B. H. Drummond, P. J. Conaghan, H. Francis, S. T. E. Jones, C. P. Grey, N. C. Greenham, D. Credgington and H. Bronstein, *J. Am. Chem. Soc.*, 2019, **141**, 18390–18394.
- X. Tang, X.-L. Li, H. Liu, Y. Gao, Y. Shen, S. Zhang, P. Lu, B. Yang, S.-J. Su and Y. Ma, *Dyes Pigm.*, 2018, **149**, 430–436.
- M. Wang, Z. Cheng, X. Meng, Y. Gao, X. Yang, H. Liu, S.-T. Zhang, H. Ma and B. Yang, *Dyes Pigm.*, 2020, **177**, 108317.
- S. Xiao, S.-T. Zhang, Y. Gao, X. Yang, H. Liu, W. Li and B. Yang, *Dyes Pigm.*, 2021, **193**, 109482.
- J. Fan, Y. Zhang, K. Zhang, J. Liu, G. Jiang, F. Li, L. Lin and C.-K. Wang, *J. Mater. Chem. C*, 2019, **7**, 8874–8887.
- J. Jiang, X. Li, M. Hanif, J. Zhou, D. Hu, S. Su, Z. Xie, Y. Gao, B. Yang and Y. Ma, *J. Mater. Chem. C*, 2017, **5**, 11053–11058.
- S.-Y. Yang, Y.-L. Zhang, A. Khan, Y.-J. Yu, S. Kumar, Z.-Q. Jiang and L.-S. Liao, *J. Mater. Chem. C*, 2020, **8**, 3079–3087.
- Y. Zhang, X. Zhou, C. Zhou, Q. Su, S. Chen, J. Song and W.-Y. Wong, *J. Mater. Chem. C*, 2020, **8**, 6851–6860.
- T. Lu and F. Chen, *J. Comput. Chem.*, 2012, **33**, 580–592.
- W. Li, Y. Pan, R. Xiao, Q. Peng, S. Zhang, D. Ma, F. Li, F. Shen, Y. Wang, B. Yang and Y. Ma, *Adv. Funct. Mater.*, 2014, **24**, 1609–1614.
- C. Lin, P. Han, S. Xiao, F. Qu, J. Yao, X. Qiao, D. Yang, Y. Dai, Q. Sun, D. Hu, A. Qin, Y. Ma, B. Z. Tang and D. Ma, *Adv. Funct. Mater.*, 2021, **31**, 2106912.
- J. Liu, Z. Li, T. Hu, X. Wei, R. Wang, X. Hu, Y. Liu, Y. Yi, Y. Yamada-Takamura, Y. Wang and P. Wang, *Adv. Opt. Mater.*, 2018, 1801190, DOI: 10.1002/adom.201801190.
- T. Liu, L. Zhu, S. Gong, C. Zhong, G. Xie, E. Mao, J. Fang, D. Ma and C. Yang, *Adv. Opt. Mater.*, 2017, **5**, 1700145.
- X. Lv, L. Xu, W. Cui, Y. Yu, H. Zhou, M. Cang, Q. Sun, Y. Pan, Y. Xu, D. Hu, S. Xue and W. Yang, *ACS Appl. Mater. Interfaces*, 2021, **13**, 970–980.
- Y. Pan, W. Li, S. Zhang, L. Yao, C. Gu, H. Xu, B. Yang and Y. Ma, *Adv. Opt. Mater.*, 2014, **2**, 510–515.
- Q. Wan, B. Zhang, Y. Ma, Z. Wang, T. Zhang and B. Z. Tang, *J. Mater. Chem. C*, 2020, **8**, 14146–14154.
- C. Wang, X. Li, Y. Pan, S. Zhang, L. Yao, Q. Bai, W. Li, P. Lu, B. Yang, S. Su and Y. Ma, *ACS Appl. Mater. Interfaces*, 2016, **8**, 3041–3049.
- C. Wang, X.-L. Li, Y. Gao, L. Wang, S. Zhang, L. Zhao, P. Lu, B. Yang, S.-J. Su and Y. Ma, *Adv. Opt. Mater.*, 2017, **5**, 1700441.
- W. Xie, B. Li, X. Cai, M. Li, Z. Qiao, X. Tang, K. Liu, C. Gu, Y. Ma and S. J. Su, *Front. Chem.*, 2019, **7**, 276.
- Y. Xu, P. Xu, D. Hu and Y. Ma, *Chem. Soc. Rev.*, 2021, **50**, 1030–1069.
- L. Yao, B. Yang and Y. Ma, *Sci. China: Chem.*, 2014, **57**, 335–345.
- Y. Zheng, X. Zhu, Z. Ni, X. Wang, Z. Zhong, X. J. Feng, Z. Zhao and H. Lu, *Adv. Opt. Mater.*, 2021, **9**, 2100965.
- Z. D. Li, B. B. Suo, Y. Zhang, Y. L. Xiao and W. J. Liu, *Mol. Phys.*, 2013, **111**, 3741–3755.
- Z. D. Li, Y. L. Xiao and W. J. Liu, *J. Chem. Phys.*, 2012, **137**, S10–S16.
- Z. D. Li, Y. L. Xiao and W. J. Liu, *J. Chem. Phys.*, 2014, **141**, 16–27.
- W. J. Liu, F. Wang and L. M. Li, *J. Theor. Comput. Chem.*, 2003, **2**, 257–272.
- F. B. Dias, T. J. Penfold and A. P. Monkman, *Methods Appl. Fluoresc.*, 2017, **5**, 012001.
- H. Liu, L. Yao, B. Li, X. Chen, Y. Gao, S. Zhang, W. Li, P. Lu, B. Yang and Y. Ma, *Chem. Commun.*, 2016, **52**, 7356–7359.
- P. K. Samanta, D. Kim, V. Coropceanu and J. L. Bredas, *J. Am. Chem. Soc.*, 2017, **139**, 4042–4051.
- C. Zhou, S. Zhang, Y. Gao, H. Liu, T. Shan, X. Liang, B. Yang and Y. Ma, *Adv. Funct. Mater.*, 2018, **28**, 1802407.
- H. J. Kim, H. Kang, J. E. Jeong, S. H. Park, C. W. Koh, C. W. Kim, H. Y. Woo, M. J. Cho, S. Park and D. H. Choi, *Adv. Funct. Mater.*, 2021, **31**, 2102588.